*J. Fluid Mech.* (1988), *vol.* 189, *pp.* 263–286
*Printed in Great Britain*



# The onset of convection and turbulence in rectangular layers of normal liquid $^4$He

By R. W. MOTSAY, K. E. ANDERSON AND R. P. BEHRINGER
Department of Physics, Duke University, Durham, NC 27706, USA

(Received 16 December 1986 and in revised form 3 September 1987)

We have carried out high-precision measurements of the heat transport in intermediate-size rectangular layers of convecting normal liquid $^4$He with Prandtl numbers of 0.52 and 0.70. The containers used for these experiments had horizontal dimensions, in units of the height $d$, of $13.4 \times 5.95$ (cell I) and $18.2 \times 8.12$ (cell II). The slopes $N_1$ of the Nusselt curves were 0.56 and 0.70 respectively for cell I and cell II. These values are significantly lower than predictions for $N_1$ for horizontally unbound layers, but comparable with results obtained in cylindrical containers of liquid helium with roughly the same number of convection rolls. For the two containers, the onset of the first instability after the onset of convection occurred at Rayleigh numbers $R_1$ that were in reasonable quantitative agreement with the predictions of Busse and Clever for the skewed-varicose instability. For both containers, the transition at $R_1$ was characterized by long transients ranging from $\sim 10^2$ to $\sim 10^3$ vertical-thermal-diffusion times. A decrease in the Nusselt number was also observed. As the Rayleigh number was increased above $R_1$, a new steady state evolved and then additional transitions were observed. These transitions occurred at Rayleigh numbers labelled $R_2, R_3, \ldots$, with a total of five transitions seen in cell I and a total of three transitions seen for cell II. The transition for each cell at $R_2$ can be related quantitatively to the skewed-varicose instability, and the transition at $R_3$ is associated with an oscillatory instability. For cell II, the time-dependence beginning at $R_3$ persisted to the highest Rayleigh number studied, $R = 11.7R_c$. However, for container I, two more regimes of time-independent flow were observed; the last of these was at an unexpectedly high Rayleigh number of $6.7R_c$. This work extends to lower Prandtl number recent studies made on moderate-size rectangular layers of convecting water and alcohol.

## 1. Introduction

### 1.1. *Overview*

Rayleigh–Bénard convection occurs when a layer of fluid with positive expansion coefficient is driven into a convective state by heating the layer from below. When convection occurs, there is a resulting flow pattern in the form of convection rolls. Although much attention has been given to this system, unresolved questions remain. (For recent reviews see Busse 1981; Normand, Pomeau & Velarde 1981; and Behringer 1985.) Two of these questions which are considered in the present work concern the effect of sidewalls on steady convection and the nature of secondary instabilities on the convective rolls leading to the onset of turbulence.

The global parameters which determine the flow are the Rayleigh number and the Prandtl number given by

$$R = \frac{\alpha_p g d^3 \Delta T}{\kappa \nu}, \tag{1}$$

and

$$Pr = \frac{\nu}{\kappa}. \tag{2}$$

Here, $a_p$ is the isobaric expansion coefficient, $\kappa$ is the thermal diffusivity, $\nu$ is the kinematic viscosity, $g$ is the acceleration due to gravity, and $d$ is the height of the layer across which a temperature difference $\Delta T$ is imposed. In addition, the geometry of the confining sidewalls may significantly affect the flow. Here, we present results for rectangular geometries. In this case the geometry is specified by $L_x \times L_y$, respectively the long and short horizontal lengths expressed in units of $d$. We shall compare our data to results obtained in cylindrical geometries for which the appropriate parameter is the aspect ratio $\Gamma$, defined by

$$\Gamma = \frac{D}{2d}, \tag{3}$$

where $D$ is the diameter of the cylindrical layer.

The fluid used in these experiments was liquid $^4$He. This fluid is particularly interesting because its easily accessible Prandtl-number range, $0.5 \lesssim Pr \lesssim 1$, overlaps the value 0.7, which is typical of room-temperature gases, and extends to roughly the range that can be obtained with room-temperature fluids. In addition, liquid helium is useful because existing cryogenic techniques permit very high-precision heat-transport measurements (Ahlers 1974; Behringer 1985).

One goal of the present experiments is to provide a comparison to predictions for the secondary instabilities in the liquid-helium Prandtl-number range. For a number of reasons, existing experiments cannot be compared directly to theory. Many of the studies of convective flows employing liquid helium (Ahlers 1974; Ahlers & Behringer 1978*a*,*b*; Ahlers & Walden 1980; Behringer *et al.* 1982; Walden 1983; Behringer, Gao & Shaumeyer 1983; Lucas, Pfotenhauer & Donnelly 1983; Pfotenhauer, Lucas & Donnelly 1984; Gao & Behringer 1984; Behringer 1985) have been carried out using cylindrical geometries. However, the patterns that form in cylindrical containers differ from the straight parallel rolls that are often considered in analytical theories (Clever & Busse 1974; Busse & Clever 1979; Bolton, Busse & Clever 1986). Those helium experiments that have used rectangular geometries (Maurer & Libchaber 1980; Maeno, Hauke & Wheatley 1985) typically have had small values of $L_x \times L_y$ in order to suppress the effects of pattern disorder. Similarly, recent experiments by Kessler, Dallman & Oertel (1984) on air ($Pr = 0.7$) were performed in a small container. Hence, these experiments have not produced conditions that are appropriate for comparing to stability theories, which assume unconfined straight rolls.

On the other hand, in a moderate-size rectangle, experiments in higher-Prandtl-number fluids by Walden *et al.* (1984) and by Kolodner *et al.* (1986), which extend older work (Chen & Whitehead 1968; Krishnamurti 1970; Willis & Deardorf 1970; Stork & Müller 1972; Krishnamurti 1973; Whitehead 1976; Busse & Clever 1979), indicate that convection rolls form that are parallel to the short side of the container. At least some aspects of the data obtained in such a geometry can be compared in a quantitative way to predictions.

In the present experiments, two rectangular containers were used with dimensions $L_x \times L_y = 13.4 \times 5.95$ (cell I) and $L_x \times L_y = 18.2 \times 8.12$ (cell II). The sizes of these containers were chosen to fall in an intermediate-size regime in anticipation that straight parallel-roll patterns would occur, and that a quantitative comparison to

| | $d$ (cm) | $L_x$ | $L_y$ | $Pr$ | $\overline{T}$ (K) |
|---|---|---|---|---|---|
| Cell I | $0.171 \pm 0.001$ | 13.4 | 5.95 | 0.70 | 2.2042 |
| Cell II | $0.125 \pm 0.001$ | 18.2 | 8.12 | 0.52 | 2.3485 |

| | $t_v$(s) | $R_c$ | $\Delta T_c$(mK) | $Q_{OB}$ (at $\Delta T_c$) |
|---|---|---|---|---|
| Cell I | 114 | $1590 \pm 280$ | 1.002 | $-0.0034$ |
| Cell II | 38.1 | $1750 \pm 200$ | 2.284 | $-0.0053$ |

TABLE 1. Characteristics of the convection containers. $\overline{T}$ is the mean temperature at the onset of convection. $Q_{OB}$ is the same as the parameter $Q$ used by Walden & Ahlers (1981), which in turn is the parameter $P$ introduced by Busse (1967) to characterize departures from the Oberbeck–Boussinesq approximation.

theory would be possible. The container sizes in dimensional units and other relevant information are given in table 1.

Our measurements are taken from heat-flow experiments, and our data are presented as a Nusselt number $N$, which is defined as the total heat flux actually carried by the layer, $Q_T$, normalized by the conductive heat flux, $Q_C$:

$$N = Q_T/Q_C. \tag{4}$$

In addition, we characterize time-dependent flows by fixing the heat flux and then observing fluctuations $\delta T$ in $\Delta T$. A convenient representation is then the dimensionless quantity $\delta T/\Delta T_c$, where $\Delta T_c$ is the value of $\Delta T$ at $R_c$, the Rayleigh number at the onset of convection.

In the remainder of this section, we shall review recent theory and experiments that are relevant to this work. Section 2 provides a description of the apparatus and a discussion of experimental techniques. We present our results in §3, and §4 contains some concluding remarks.

### 1.2. *Review of recent theory and experiment*

Fluids such as liquid $^4$He or air have a stability diagram with the features given in figure 1, which follows the work of Clever & Busse (1974) and Busse & Clever (1979). Here, the stability of a horizontally infinite layer of straight parallel convection rolls to infinitesimal perturbations is given in terms of the Rayleigh number $R$ and the dimensionless roll wavevector $\alpha$. Within the region enclosed by the lines labelled O, E, and SV, straight parallel convection rolls are expected to be stable to infinitesimal perturbations. These lines indicate when the oscillatory (O), Eckhaus (E), and skewed-varicose (SV) instabilities will first occur.

In particular, if straight parallel rolls with wavenumber $\alpha_c$ were generated in a fluid like liquid helium, and if $R$ were increased gradually from $R_c$, the skewed-varicose-instability (SVI) boundary would be encountered. Existing theory for a horizontally infinite layer considers only linear order in the perturbations and ignores the effects of rigid sidewalls; thus it does not indicate what would happen following an increase in $R$ above the SVI boundary. Calculations have been carried out for small-$L$ containers, $L \lesssim 4$, by several authors, including Kessler (1987), Kessler *et al.* (1984), and Yahata (1986, 1988). Of some interest here are the predictions made for the onset of time dependence. Kessler *et al.* find that the onset of time dependence for a rectangular layer of fluid having $Pr = 0.71$ and $L_x \times L_y = 4 \times 2$ occurs via an

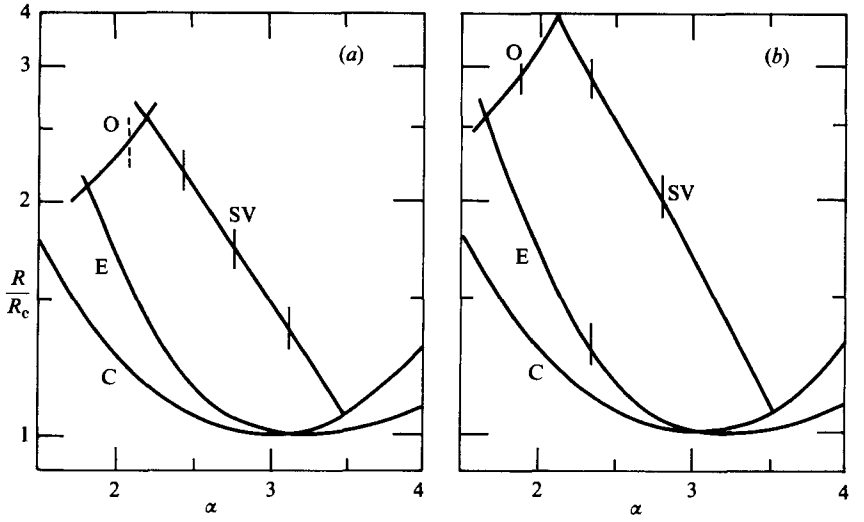


FIGURE 1. Stability diagrams for the two Prandtl numbers used in our experiments, after Busse & Clever (1979): (*a*) $Pr = 0.52$ (cell II), (*b*) $Pr = 0.70$ (cell I). The small vertical lines indicate estimates of the wavevectors which occur in cell II (*a*) and cell I (*b*). The stable region for straight parallel rolls is bounded by the stability curves marked O (oscillatory), E (Eckhaus), and SV (skewed varicose). The curve C is the stability boundary for the onset of convection.

oscillatory instability. Yahata has identified both an oscillatory instability via a Hopf bifurcation and a real-eigenvalue mode which can also lead to periodic time dependence of the type found in cylindrical containers of argon and liquid helium, as discussed below. The time dependence that we find at the first instability is qualitatively different from what both sets of authors find, as discussed below.

Information on the dynamics near the instability boundaries, and in particular the SVI boundary, has been obtained from recent experiments, both in liquid helium (Maurer & Libchaber 1980; Behringer *et al.* 1983; Gao & Behringer 1984) and in room-temperature fluids (Gollub & Steinman 1981; Gollub, McCarrier & Steinman 1982; Walden *et al.* 1984; Pocheau, Croquette & Le Gal 1985; Kolodner *et al.* 1986). Even for horizontally large layers, the vertical boundaries may significantly affect the way in which the instabilities, and in particular, the SVI are manifested. To show this we review three types of recent experiments.

(*a*) *Large rectangular containers*: Gollub & Steinman (1981) and Gollub *et al.* (1982) have found that for large rectangles of water ($L_x \times L_y = 30 \times 20$; $Pr = 2.5$) non-parallel convection rolls form in the absence of an appropriate external forcing effect, a result which has been explained by Cross (1982). Because the SVI depends strongly on $\alpha$, the instability apparently occurs locally in such a flow pattern.

(*b*) *Cylindrical containers*: The SVI has also been found to play a role in lower-$Pr$ measurements made in cylindrical containers. These measurements include studies by Pocheau *et al.* (1985) using argon ($Pr = 0.71$) with flow visualization, and high-precision thermal measurements by Behringer *et al.* (1983) and by Gao & Behringer (1984) using liquid $^4$He. For a cylindrical layer, an instability related to the SVI occurs at $R_1$, with $R_1 \approx 1.15$ when $\Gamma \approx 7.5$. For such an aspect ratio, the number of convection rolls should be roughly comparable with that in either of the present containers. This low value, $R_1 \approx 1.15$, has been explained by Pocheau *et al.* (1985) who found that the instability at $R_1$ occurs as a local manifestation of the SVI in the

curved non-uniform rolls that exist above $R_c$. Behringer *et al.* (1983) and Gao & Behringer (1984) showed that when the instability was encountered, periodic motion ensued which was usually characterized by a finite amplitude and a frequency $f$, which vanished at the onset Rayleigh number $R_1$ as $f \sim (R-R_1)^{\frac{1}{2}}$. G. Metcalfe and D. G. Schaeffer (private communication) have discussed why the SVI should be modified in cylindrical containers to produce the observed periodic behaviour.

(*c*) *Moderate-size rectangular containers*: Of particular importance to this work are flow visualizations in moderate-size rectangular layers of water or ethanol ($2 \lesssim Pr \lesssim 20$) by Walden *et al.* (1984) and by Kolodner *et al.* (1986). Using containers with $L_x \times L_y \approx 10 \times 5$, they found rolls parallel to the short side of the container just above $R_c$. If the Rayleigh number was increased, the original rolls lost stability at a wavevector and Rayleigh number that corresponded reasonably well with the predictions for the SVI or, where appropriate, the knot instability (KI), an instability that is not relevant for liquid-helium Prandtl numbers. After a fairly short time, of order $t_v$, the vertical thermal diffusion time, defined by

$$t_v = d^2/\kappa, \tag{5}$$

the rolls reformed with a smaller mean wavevector. Thus, the SVI was manifested in a moderate-size container as a wavenumber reduction mechanism as a consequence of the negative slopes of the SVI and KI curves. If the Rayleigh number was increased further, then the SVI or KI boundary was again encountered. Yet another decrease in the number of convection rolls, with a corresponding decrease in $\alpha$ occurred. The reduction of the wavevector was found to occur until a stability boundary with positive slope, the knot instability (Clever & Busse 1974; Busse & Clever 1979; Bolton *et al.* 1986), was encountered. At this point, further wavenumber reduction was no longer possible, parallel rolls ceased to be stable, and the flow was no longer steady in time.

Although the flow patterns in liquid-helium experiments have not yet been directly observed, we expect that the convective rolls in the present rectangular containers are most likely to form a parallel-roll pattern with an average wavevector close to the infinite-layer prediction $\alpha_c = 3.117$. Additional evidence for this assumption is given in the work of Kessler *et al.* (1984). Using air in a small rectangular container with dimensions $L_x \times L_y = 4 \times 2$, they found convection rolls aligned with the short side. With increasing $R$, a set of transitions was observed. In this case, the transitions were clearly associated with changes in the number of convection rolls, but the Rayleigh numbers at which the transitions occurred were substantially higher than the predictions of Busse & Clever (1979) for the SVI. The latter fact is attributable to the strong influence of the sidewalls in their small-$L$ experiment.

We estimate that the wavevector in the present experiments will be

$$\alpha \approx \frac{2\pi}{L_x n}, \tag{6}$$

where $n$ is the number of roll pairs and $L_x$ is the long dimension, expressed in units of $d$. The most likely value of $n$ near $R_c$ should make $\alpha$ as close as possible to $\alpha_c$. For cell II, $n = 9$ yields $\alpha = 3.11$, a value quite close to the preferred one. We expect that the SVI will be encountered at near critical wavevectors; i.e. from figure 1, near $R/R_c = 1.37$. For cell I the situation is more complicated; the choice $n = 6$ yields $\alpha = 2.81$, and the choice $n = 7$ yields $\alpha = 3.28$. These two values of $\alpha$ bracket the

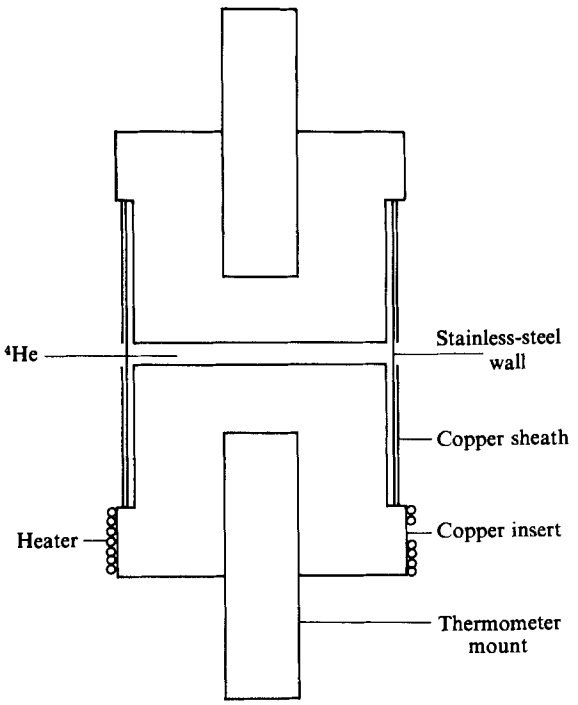


FIGURE 2. Scale drawing depicting the long side of the rectangular containers used in this experiment.

'optimum' choice, $\alpha_c$, with comparable critical Rayleigh numbers, and it is not clear which value of $n$ is preferred or whether an odd number of rolls will form. The SVI boundary occurs for the Prandtl numbers of interest at $R = 2.0R_c$ for $\alpha = 2.81$, and at $1.3R_c$ for $\alpha = 3.28$. As discussed below, the experiments indicate that $n = 6$ is the most reasonable choice.

## 2. Apparatus and experimental procedure

The experiments were carried out in a cryostat similar to that described by Behringer & Ahlers (1982), and the interested reader is referred to that work for more details. Aside from their rectangular geometry, the containers, shown in cross-section in figure 2, are qualitatively similar to other cryogenic containers having circular cross-sections (Behringer & Ahlers 1982; Gao *et al.* 1987). In particular, the faces of these containers were made of OFHC copper parallelopipeds. The surfaces forming the fluid boundaries were lapped to an optically reflecting finish. Using an optical flat and a monochromatic light source, we determined that the faces were flat to between $2\lambda$ and $4\lambda$, where $\lambda \approx 6000$ Å was the wavelength of the light source. The estimated variation of $d$ for each cell is given in table 1. The sidewalls were made of thin stainless steel (wall thickness = 0.015 cm). In order to keep these walls at the same temperature as the interior copper plugs forming the horizontal boundaries, strips of copper were attached to the outside and to the base of the plugs using Emerson and Cummings 1266 epoxy.

As in previous cryogenic experiments, we used the heat flux $Q$ as the independent parameter; the Rayleigh number was then determined by measuring $\Delta T$ at fixed $Q$

and at a fixed top temperature. We obtained $\Delta T$ using differential germanium resistance thermometry. By fixing $Q$ rather than $\Delta T$, we obtained precise data with considerably more facility than we would have obtained by fixing $\Delta T$ and measuring $Q$; the equivalence of the two methods in the context of this type of experiment has been demonstrated elsewhere (Gao & Behringer 1984). Near the onset of convection, measurements were made by first fixing the top temperature, setting $\Delta T$ to a value near $\Delta T_c$, and then increasing or decreasing $Q$ by small steps. Typically, five or six steps were made, and then $Q$ was set to zero or some other convenient reference value to check for possible thermometry drifts. After each small step, the system was allowed to equilibrate for times of order $10t_v$ to $20t_v$. Typical step sizes were between $0.01Q_c$ and $0.05Q_c$, where $Q_c$ is the value of $Q$ at $R_c$. In the region near $R_c$, where steady convection was obtainable, no dependence on step size or direction was seen.

All the data were obtained with liquid $^4$He at saturated vapour pressure. The top boundary of the fluid was held at a fixed temperature which was unique to each container. For cell I this temperature was 2.2042 K; for cell II it was 2.3485 K. Hence, the Prandtl numbers were somewhat different for the two containers. For cell I, $P = 0.70$, and for cell II, $P = 0.52$. These values were obtained from the data tabulated by Barenghi, Donnelly & Lucas (1981), and evaluated at the mean temperature of each layer when $R$ was at its critical value. The relatively small difference in $P$, 0.52 versus 0.70, has a moderately strong effect on the stability diagram. Thus, figure 1 (*b*) shows the stability diagram for $P = 0.70$ (the case for cell I) and figure 1 (*a*) shows the stability diagram for $P = 0.52$ (the case for cell II).

An additional consideration is the temperature variation of the fluid parameters such as the viscosity, etc. In the usual Oberbeck–Boussinesq approximation, these quantities are assumed constant. The effect of departures from the Oberbeck–Boussinesq approximation has been considered theoretically by Busse (1967) and experimentally by Walden & Ahlers (1981). A useful parameter for considering departures from this approximation is Busse's parameter $P$, which was also denoted by $Q$ in the work of Walden & Ahlers. To avoid confusion with other symbols used in this work, we shall use $Q_{OB}$ for this quantity. Estimates of $Q_{OB}$ for our two cells at the onset of convection are given in table 1. From these estimates, we conclude that non-Boussinesq effects are not a serious consideration for this work.

As a final point in this section, we note that in the discussion below we often use $R_c$ as a convenient normalization for the Rayleigh numbers of interest. In the absence of temperature variations of the thermo-hydrodynamic parameters contained in the Rayleigh number, the ratio $R/R_c$ is equivalent to the ratio of the temperature difference $\Delta T$ to the temperature difference $\Delta T_c$. Here, $\Delta T$ is the temperature difference at $R$, and $\Delta T_c$ is the temperature difference at $R_c$. Throughout this work, we have corrected for temperature variations in the fluid parameters so that values of $R/R_c$ are not simply the ratio $\Delta T/\Delta T_c$.

## 3. Results

### 3.1. *Summary*

We first provide a brief summary of our findings which we then develop more fully in the rest of this section. Briefly, we find that:

(*a*) For rectangular layers, there is a Rayleigh-number regime above the onset of convection, $R_c < R < R_1$ for which heat-transport measurements with a precision of $\approx 0.03\,\%$ indicate steady convective flow. Below the onset of the instability at $R_1$,

| | Cell I | Cell II |
|---|---|---|
| $R_a/R_c$ | — | 1.22 |
| $R_1/R_c$ | 2.29 | 1.42 |
| $R_1^*/R_c$ | 2.38 | 1.74 |
| $R_2/R_c$ | 2.87 | 1.88 |
| $R_2^*/R_c$ | 3.02 | 2.03 |
| $R_3/R_c$ | 3.39 | 2.53 ( $= R_t$) |
| $R_3^*/R_c$ | 3.85 | — |
| $R_4/R_c$ | 4.06 | — |
| $R_4^*/R_c$ | 6.68 | — |
| $R_5/R_c$ | 7.14 ( $= R_t$) | — |

TABLE 2. Transition Rayleigh numbers for cells I and II

the Nusselt curves, which are shown in figures 3 and 4 for the two containers studied here, evolve smoothly as functions of $R$ (with a slight exception for cell II). At $R_1$, the initial flow patterns lose stability. It seems likely that the flow patterns also evolve smoothly with increasing $R$ up to $R_1$, with again a slight exception in the case of cell II. Measurements (Behringer *et al.* 1983; Gao & Behringer 1984) on cylindrical containers of liquid helium also indicate steady flow between $R_c$ and an appropriate $R_1$, but:

(*b*) The value $R_1$ of $R$ at which the initial flow pattern loses stability is significantly higher for the present rectangular containers than for those with a circular cross-section. The present values of $R_1$ are slightly higher than predictions for the SVI. We attribute this difference to finite-size effects, and we conclude that our results are essentially in agreement with theory. Specifically, $R_1 = 2.29R_c$ for cell I, whereas we expect $R_1 = 2.0R_c$ from theory. For cell II, there is a small reproducible increase in the Nusselt curve at $R_a = 1.22R_c$ indicating a small pattern adjustment. However, the first major change occurs at $R_1 = 1.42R_c$, which is to be compared with the expected value $R_1 = 1.37R_c$.

(*c*) Long transients are seen just above $R_1$, in both cells I and II, but particularly for the latter. For both containers, there is a value of $R$, $R_1^*$, with $R_1^* > R_1$, for which no long transients are seen and steady flow is obtained after relatively short equilibration times.

(*d*) There are still higher Rayleigh numbers $R_2$, $R_3$, and for cell I, an $R_4$ and $R_5$ at which steady rapidly equilibrating flow yields to very long transients and/or time dependence, with steady flow reappearing at $R_i^*$ where $R_i < R_i^* < R_{i+1}$. Thus, transients/time dependence starting at $R_2$ stop at $R_2^*$. The values of $R_1, R_2, \ldots$ are indicated for each container in table 2. Up to $R_3$, the observed transition Rayleigh numbers are in agreement with theory and expectations for the wavenumber, and these results are similar to observations in higher-Prandtl-number fluids. For cell I there are some additional transitions which do not fit simply into the current understanding.

(*e*) The values $R_1, R_2, \ldots$ are reproducible within about $\pm 0.05R_c$, whereas the type of transient/time dependence seen just above each of these Rayleigh numbers is not necessarily exactly reproducible.

(*f*) There is a Rayleigh number $R_t$ at which persistent time dependence sets in; for $R > R_t$, no steady flow is seen.

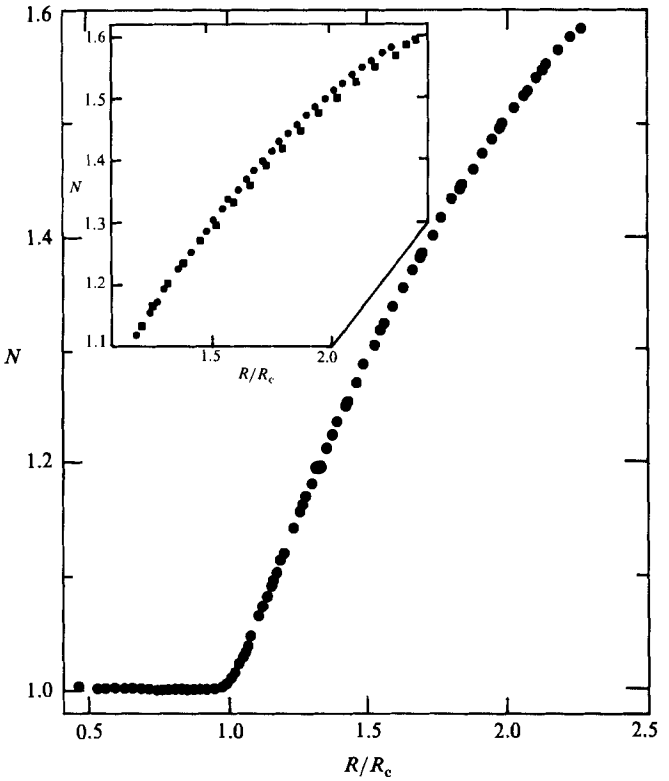


FIGURE 3. Nusselt number *vs.* Rayleigh number near the onset of convection and up to $R_1$ for cell I. Inset: Nusselt number for cell I *vs.* $R/R_c$. ●, increasing Rayleigh number; ■, decreasing Rayleigh number following the transition to a new roll pattern at $R_1$.

### 3.2. *Steady flow near* $R_c$

We now discuss these points in more detail starting with the results near $R_c$. Figures 3 and 4 show heat-transport curves near the onset of convection and up to $R_1$ for cells I and II respectively.† The critical values of the Rayleigh number were determined from the values of $\Delta T_c$, the measured result for $\Delta T$ at the onset of convection, as given in table 1, and from the thermohydrodynamic data tabulated by Barenghi *et al.* (1981). We obtained $R_c = 1590 \pm 280$ for cell I, and $R_c = 1750 \pm 200$ for cell II. Our data overlap the infinite-layer prediction $R_c = 1708$. To our knowledge, there are no predictions of $R_c$ for rectangles comparable to those used in our experiments. However, we expect from Ahlers *et al.* (1981) and from Cross *et al.* (1983) that finite-size effects will provide a fractional correction of order $L_x^{-2}$ – too small to be detectable here because of the relatively large uncertainty in the fluid parameters.

Convection is signalled by the initial rise of $N$ above unity at $R_c$. The slope,

$$N_1 = R_c \frac{dN}{dR}, \tag{7}$$

for $R$ just bigger than $R_c$ is 0.56 for cell I and 0.70 for cell II.

These results for $N_1$ were obtained by fitting to linear and quadratic polynomials

† A tabulation of the data may be obtained from R.P.B.

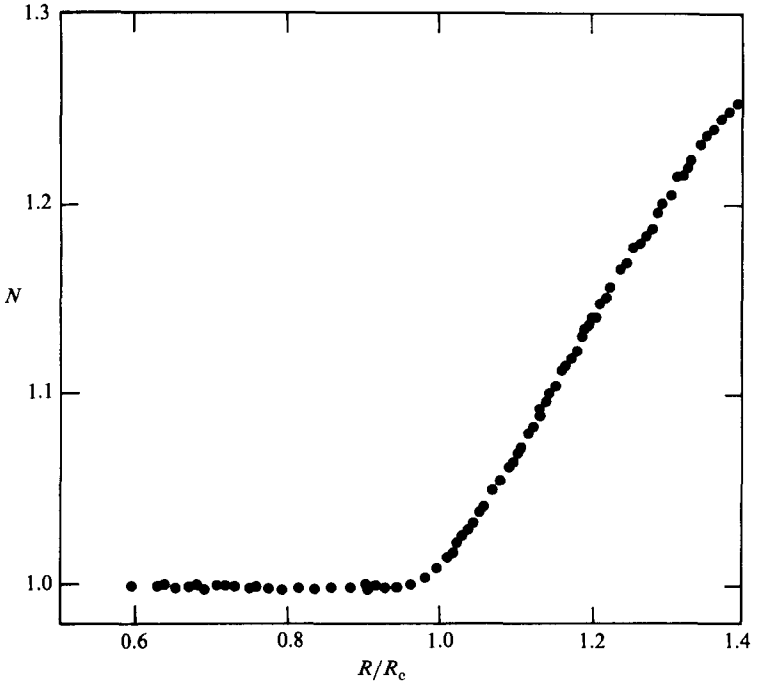


FIGURE 4. Nusselt number *vs.* Rayleigh number near the onset of convection and up to $R_1$ for cell II.

in $\Delta T$. Provided that the rounded region near $R_c$ was excluded and that only Rayleigh numbers up to $\sim 1.2R_c$ were included, the fitted slopes did not depend significantly on whether a quadratic or linear fit was used.

Owing to the presence of sidewalls, the data for $N_1$ are lower than the prediction

$$N_{1\infty} = (0.69942 - 0.00472\,Pr^{-1} + 0.00832\,Pr^{-2})^{-1}, \tag{8}$$

given by Schlüter, Lortz & Busse (1965) for a horizontally infinite layer of straight parallel rolls. Specifically, for the Prandtl numbers of these experiments, $N_{1\infty} = 1.4$. To our knowledge, there are no data of comparable Prandtl number obtained in rectangular containers with which to make comparison. However, data for a room-temperature fluid (water) in a rectangle (Ahlers & Rehberg 1986) and for cylindrically confined liquid helium (Gao *et al.* 1987) have been reported. In order to make a comparison between the room-temperature results and our own, we adjusted the former for Prandtl-number effects using (8). In figure 5, we have compared our results to the data of other experiments. We have presented the data for rectangles as a function of $\frac{1}{2}L_x$, and the results of Gao *et al.* (1987) for cylindrical containers of liquid helium as a function of $\Gamma$. Hence, containers of roughly comparable numbers of convection rolls will be compared, regardless of the geometry. The data of Gao *et al.* are represented by solid lines at low $\Gamma$ and by filled circles at high $\Gamma$. The changes with $\Gamma$ in the number of convection rolls present in the cylinders is evident. There is qualitative similarity between the results for cylinders and rectangles, although $N_1$ for the rectangles may be increasing more rapidly with $\frac{1}{2}L_x$ than does $N_1(\Gamma)$ for the cylinders. There are, to our knowledge, no calculations that predict the effect on the Nusselt number of sidewalls in a rectangular container with rigid boundaries and horizontal dimensions and Prandtl numbers appropriate to our experiments.

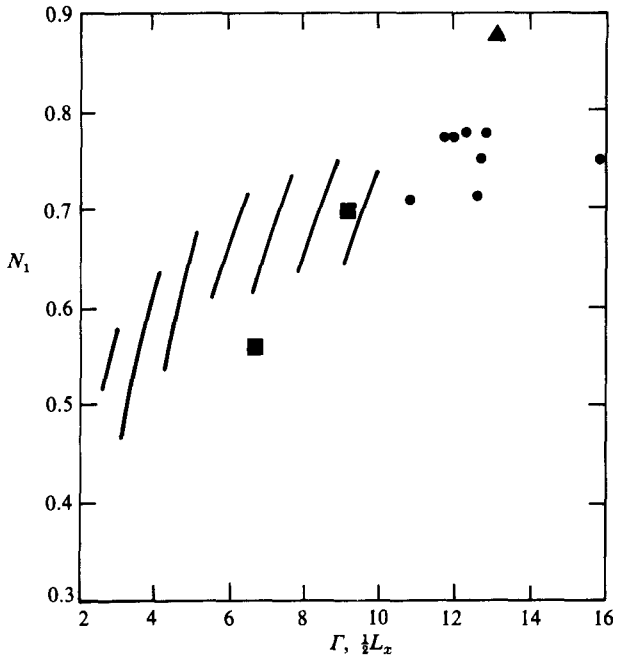


FIGURE 5. A comparison of the slopes $N_1$ found for the present rectangular containers, another rectangular container using a room-temperature fluid (water, $Pr = 6$), and recent results obtained with cylindrical containers of liquid helium. Results for rectangular containers are shown as a function of $\frac{1}{2}L_x$. Those for cylindrical containers are shown as a function of aspect ratio $\Gamma$. ■, results of the present experiments; ▲, the result $N_1 = 0.90$ of Ahlers & Rehberg (1985) for a rectangular layer of water with a correction made for Prandtl number using (8); ●, the results of Gao *et al.* (1987) for cylindrically confined layers of liquid helium, where the solid lines indicate in a summary fashion results for about 40 aspect ratios.

At $R = 1.22R_c$, the heat transport for cell II showed a small discontinuity, about 0.005 in $N$, which was found to be completely reproducible. The time-evolution of $\Delta T$ following a step increase in $Q$ from a value just below to a value just above the discontinuity, is shown in figure 6. Here, as in later figures, time variations $\delta T$ in $\Delta T$ are normalized by the value $\Delta T_c$ of the temperature difference at the onset of convection. The effect of this small transition is not particularly pronounced on the scale of figure 4. We note that no similar effect was seen in cell I. Since $R = 1.22R_c$ is not near any stability boundary for $\alpha \sim \alpha_c$, we surmize that an imperfection routinely formed in the convection rolls of cell II, and that some adjustment in the imperfection was responsible for the observed effect on the heat transport. That is, we assume that this effect is not associated with the SVI on straight parallel rolls. Our assumption is further supported by the fact that the Nusselt curve increases slightly as $R$ is increased through $R_a$. On encountering the SVI we expect the wavenumber to decrease, an event that would cause $N$ to decrease, according to Busse & Clever (1979).

In the Nusselt curves of figures 3 and 4, there is rounding apparent over a range of $\approx 0.05R_c$. The rounding in these experiments is comparable with what was observed in cylindrically confined layers of liquid helium by Gao *et al.* (1987). In other liquid-helium measurements with cylindrical containers (Behringer & Ahlers 1982) the rounded region was smaller, $\approx 0.01R_c$ to $\approx 0.02R_c$. Possible causes for the

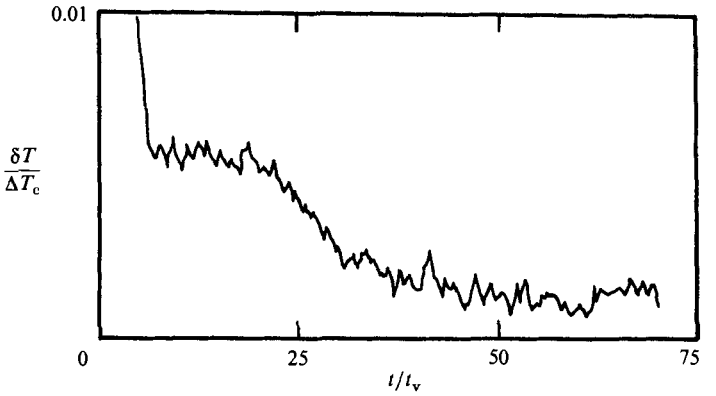


FIGURE 6. A time series showing the relaxation of the temperature difference $\Delta T$ just above $R_a = 1.22R_c$ in cell II. Here, the heat current has been increased by an amount corresponding to about $0.02R_c$ and then held constant. The variations $\delta T$ of $\Delta T$ are scaled by $\Delta T_c$, the value of $\Delta T$ at the onset of convection; time is expressed in units of $t_v$, the vertical diffusion time.

rounding may be imperfections in the spacing $d$ of the layer or imperfect thermal conditions at the vertical boundaries. However, the non-uniformities in $d$ are about the same for the present experiments and those of Behringer & Ahlers (1982) (see also table 1). A quantitative description of non-uniformities associated with thermal conditions at the boundaries is very difficult. Hence, the present data cannot provide convincing evidence for the origin of the rounding.

### 3.3. *Instabilities and the onset of time-dependence*

#### 3.3.1. *The transition at* $R_1$

The values of $R_1$ found for the two cells can be understood in terms of the predicted SVI stability boundary and reasonable assumptions for the mean wavevector. For cell II, the observed value of $R_1 = 1.42R_c$ is in good agreement with the infinite-parallel-roll prediction of $1.37R_c$ if $Pr = 0.52$ and $\alpha = 3.11$ (which we expect to be nearly the case for this container). For cell I, the first transition at $R_1 = 2.29$ indicates that the average wavevector is fairly small. As in §1, if we assume six roll pairs corresponding to an average wavevector of 2.81, we would expect from the predictions of Busse & Clever (1979), that the SVI would occur at $2.0R_c$, which is 13% lower than the observed value. It is not surprising that for a moderate-size container such as cell I, the stability boundary would occur at somewhat higher $R$ than predictions for an unbounded layer.

The transition at $R_1$ in both cells is characterized by long transients for $R$ just bigger than $R_1$. Examples are given in figure 7. Specifically, between $R_1$ and a Rayleigh number $R_1^*$, given for each container in table 2, long-term transient behaviour was observed. The time needed to obtain equilibrium just above $R_1$ for cell II ranged from a few hours ($\approx 10^2 t_v$) to, in one case, about 20 hours ($\approx 10^3 t_v$). For cell I, the transients tended to be somewhat shorter. For both containers, once $R_1^*$ was exceeded, steady flow was again obtainable with time constants of a few $t_v$. Figure 7(*a*) shows a long transient for cell I when $R$ is just greater than $R_1$, and 7(*b*) shows results just above $R_1$ for cell II. In each part of the figure, the time evolution of $\Delta T$ is given following an increase of $Q$ by an amount corresponding to a change in Rayleigh number of about $0.03R_c$. The analysis using figure 1 and (6) suggests that above $R_1^*$ the roll wavevectors have decreased to values of about 2.34 for cell I

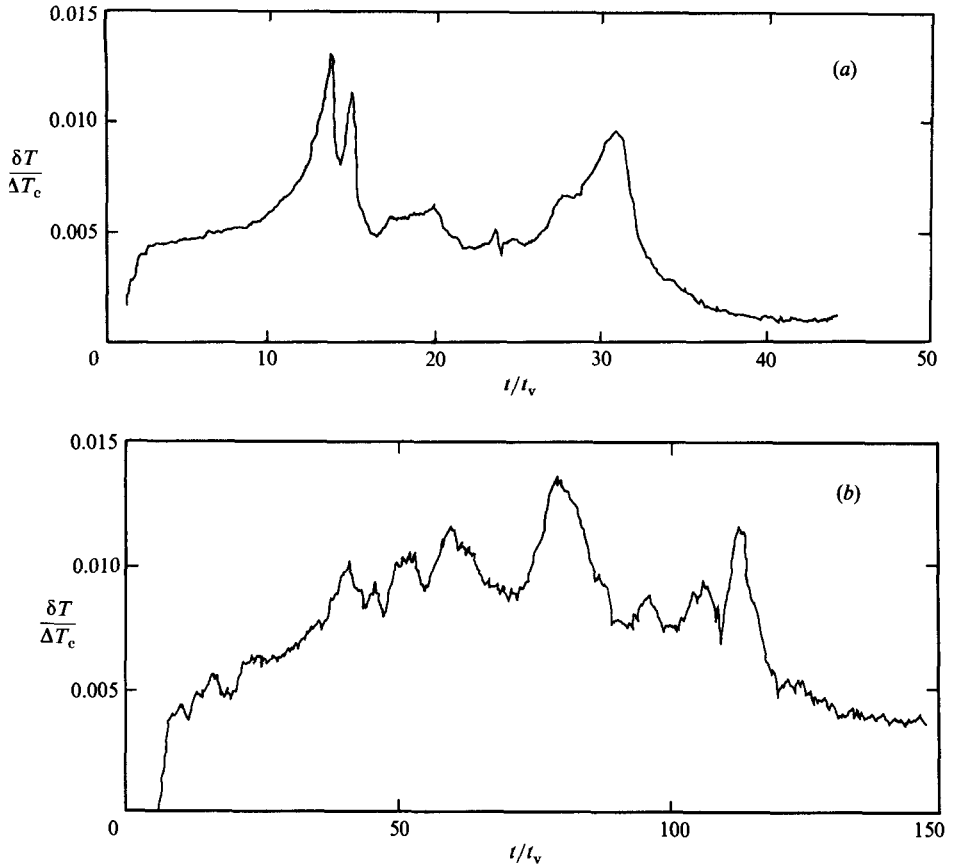


FIGURE 7. Transients occurring just above (*a*) $R_1 = 2.29R_c$ for cell I and (*b*) $R_1 = 1.42R_c$ for cell II. The time series show $\delta T/\Delta T_c$ *vs.* $t/t_v$ at fixed heat flux following a small increase in the heat flux from just below to just above $R_1$.

(corresponding to 5 roll pairs) and 2.76 for cell II (corresponding to eight roll pairs).

If after reaching a steady state above $R_1$ the Rayleigh number was slowly decreased, the Nusselt number followed a different curve from that obtained with increasing $R$. This is demonstrated in figure 3-inset for cell I. In this case, when $R$ was lowered to $1.48R_c \pm 0.06R_c$, a transition occurred and the Nusselt number returned to the curve that was obtained with increasing $R$. We associate this transition with the Eckhaus instability (see figure 1). If the Rayleigh number is decreased from within the stable region at $\alpha = 2.3$, the Eckhaus instability is predicted to occur at $1.28R_c$. Assuming that at $R_1$ for cell I the wavenumber changes from 2.81 to 2.34, we would have expected from the calculations of Clever & Busse (1974) that $N$ would have decreased by about 0.09. However, the observed decrease in $N$ is considerably smaller, about 0.03. Thus, our results in this case are qualitatively, but not quantitatively in agreement with predictions.

Our observations are similar in a number of ways to behaviour reported by Kolodner *et al.* (1986) for somewhat smaller rectangular layers ($L_x \times L_y \approx 10 \times 5$) of water. Using flow-visualization techniques, these authors found that the number of convection rolls decreased rapidly on reaching a point corresponding to the SVI

boundary or the KI boundary. When the wavevector decreased, the system was returned to a point within the stable region, where a steady parallel-roll convection pattern was again found. It seems likely that the flow in our container behaves similarly. However, there is an interesting difference between our observations and those of Kolodner *et al.* The latter found that the SVI-induced, or in some cases KI-induced, reduction in the number of rolls occurred rapidly – in a few vertical diffusion times. Yet, in our experiments, this adjustment process was very slow and characterized by long transients over a range of Rayleigh numbers near the transition. Although we do not yet have an explanation for this difference in relaxation rates, the larger horizontal dimensions of our containers versus those of Kolodner *et al.* should be noted.

Kolodner *et al.* could generate either an even or odd number of convection rolls at a given Rayleigh number. From the reproducibility of our observated values of the $R_i$, we infer that the number of convection rolls at a given Rayleigh number was always the same. This seems likely since, in our experiments, the convective states were always prepared in the same manner – by small step increases in $Q$, with time for equilibration after each step. An interpretation of our data is most reasonable if we assume that there were always an even number of rolls in both containers.

### 3.3.2. *The transition at $R_2$*

As $R$ was increased above $R_1^*$, we found that a regime of steady flow gave way at $R_2$ to a new instability. From (6) figure 1, and our previous observations of $R_1$, we would expect transitions at $2.86R_c$ and $1.76R_c$ for cells I and II respectively. These estimates are quite close to the observed values of $R_2$, namely for cell I, $R_c = 2.87R_c$, and for cell II, $R_2 = 1.88R_c$. Referring to figure 1, we would expect that above $R_2$ the pattern for cell I would consist of four roll pairs corresponding to a wavevector of 1.88, and the pattern for cell II would consist of seven roll pairs corresponding to a wavevector of 2.42.

The dynamics near $R_2$ were found to be different for the two containers as demonstrated by figure 8. For cell I long transients were seen which decayed to a steady state. For cell II, an apparently robust periodic flow was observed. In either case, the dynamics that we observe are significantly different from the rapid decrease in roll number reported by Kolodner *et al.* (1986).

For both cell I and cell II there was a region above $R_2$ for which steady flow was obtained. This new regime of steady flow began at a Rayleigh number $R_2^*$, given for each container in table 2.

### 3.3.3. *Oscillatory instability, additional transitions and the onset of turbulence*

For cell II, the steady-flow regime starting at $R_2^*$ was the last encountered as $R$ was increased; at $R = R_3 = R_t = 2.53R_c$, periodic time dependence was encountered (figure 9*a*). This periodic flow seen in cell II persisted for only a short range in $R$, and then was supplanted by non-periodic flow beginning at $2.87R_c$ (figure 9*b*). The flow remained non-periodic up to $R = 11.7R_c$, the maximum Rayleigh number for cell II that we could reach with the present apparatus. Power spectra for the two time series of figure 9 are given in figure 10, where the frequencies have been expressed in units of $t_v^{-1}$. Here, the power is calculated from variations $\delta T(t)$ of $\Delta T$ with $\delta T$ normalized by $\Delta T_c$. Although a transition to periodic flow associated with the oscillatory instability might reasonably occur at the observed $R_t$ of cell II, the experiment is characterized by a frequency that is small compared to what is indicated by the calculations of Clever and Busse. Using an estimated wavevector $\alpha \approx 2.1$, these

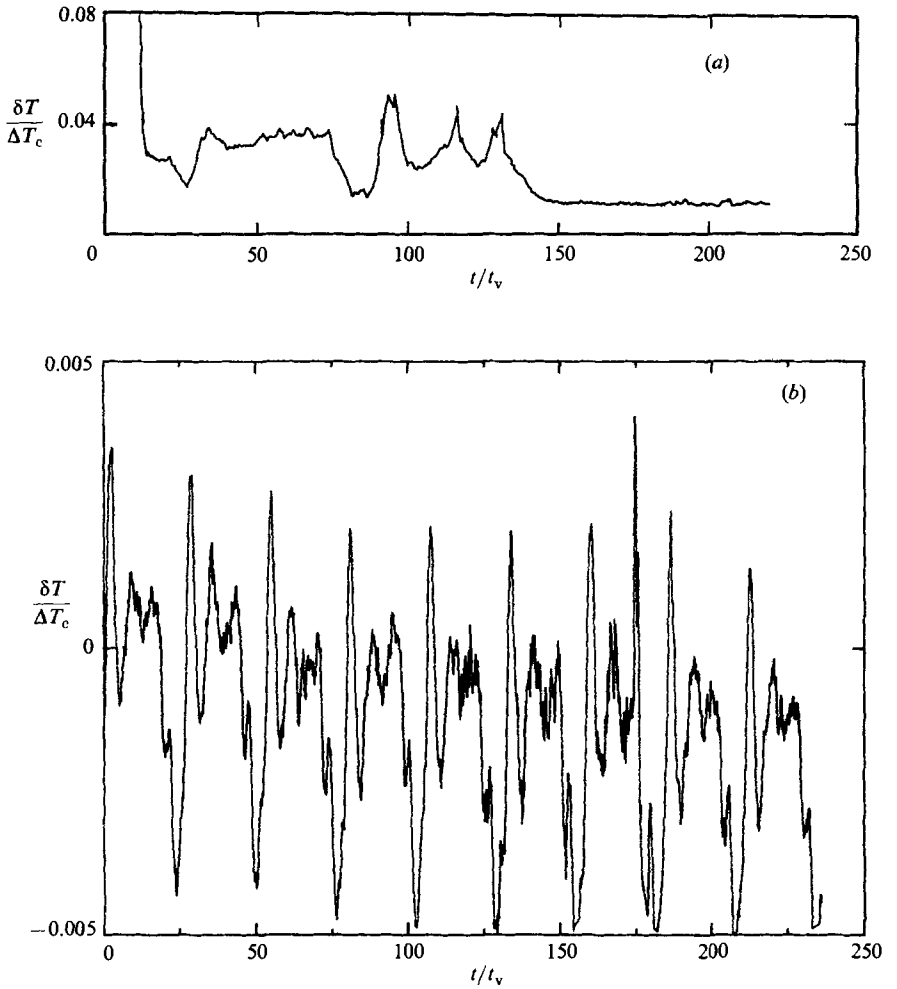


FIGURE 8. Time series similar to those shown in figure 7, but for the transition at $R_2$: (*a*) cell I; (*b*) cell II.

calculations indicate a frequency $f$ for the fastest-growing oscillatory mode of $ft_v \gtrsim 2$. The experimental value is $ft_v = 1.55 \times 10^{-1}$. In regard to the difference in the predicted and observed frequencies, we note that the predictions apply to horizontally unbounded layers. The instabilities are expected to occur with wavevectors that are transverse to the original convection rolls. In the experiments, this direction corresponds to the short dimension of the container, and the instability may be significantly affected by finite-size effects. Alternatively, Walden *et al.* (1984) have found that when the wavevector and the Rayleigh number are near the intersection point of two instabilities, such as the SVI and oscillatory instability, the resulting dynamics may not correspond to what is expected for either type of mode. We note that in figure 10(*a*) there is a slight knee at $ft_v \approx 3$, which is a frequency appropriate to the oscillatory instability. The non-periodic flow found in cell II above the periodic state is characterized by a broadband spectrum (figure 10*b*). The predicted oscillatory instability frequency for $\alpha = 2.1$ does not fall close to any feature in the spectrum of figure 10(*b*).

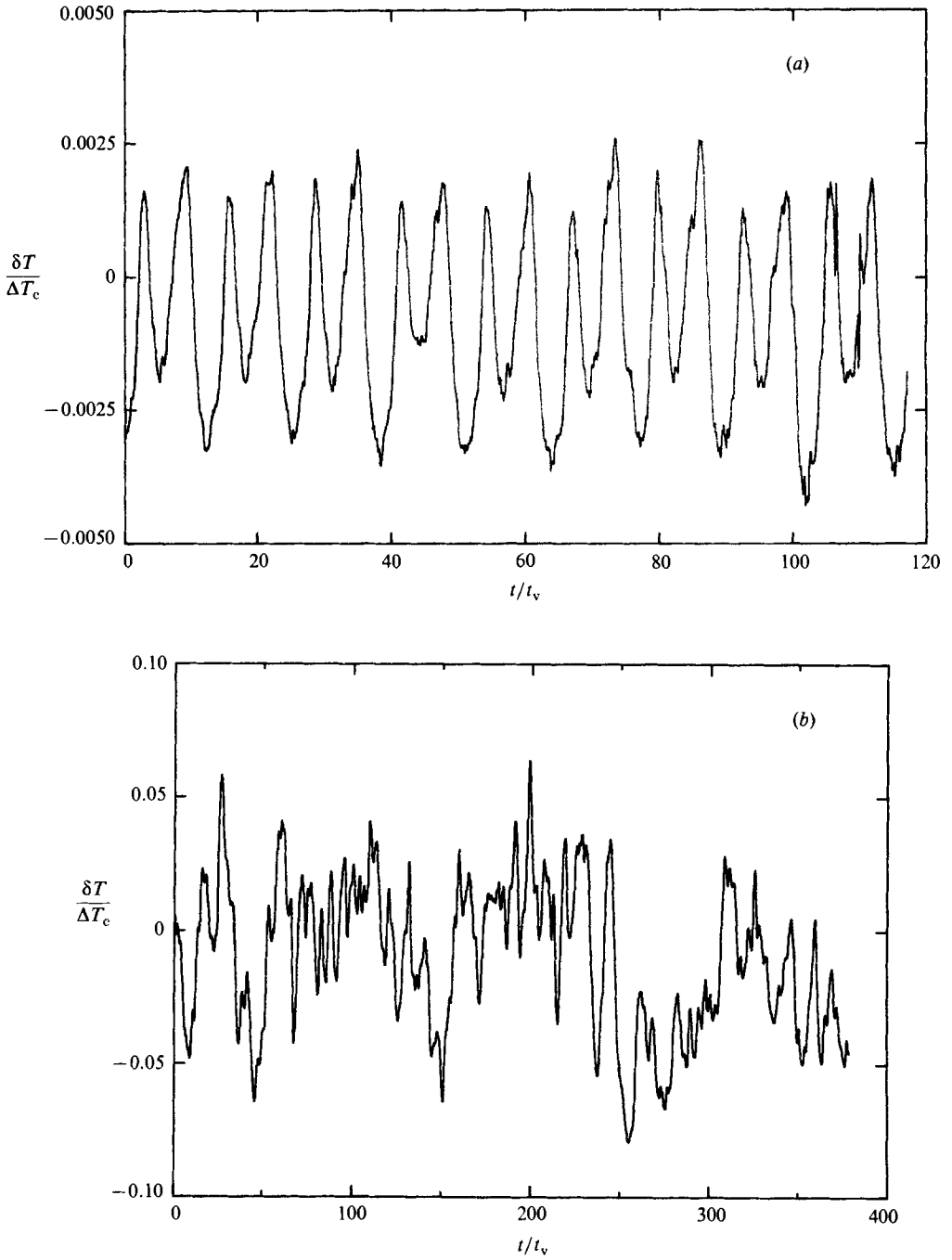


FIGURE 9. Time series near $R_3$ for cell II. (*a*) Periodic oscillations following a transient for $R = 2.53R_c$; (*b*) The non-periodic flow that evolves at a somewhat higher Rayleigh number, $R = 2.87R_c$.

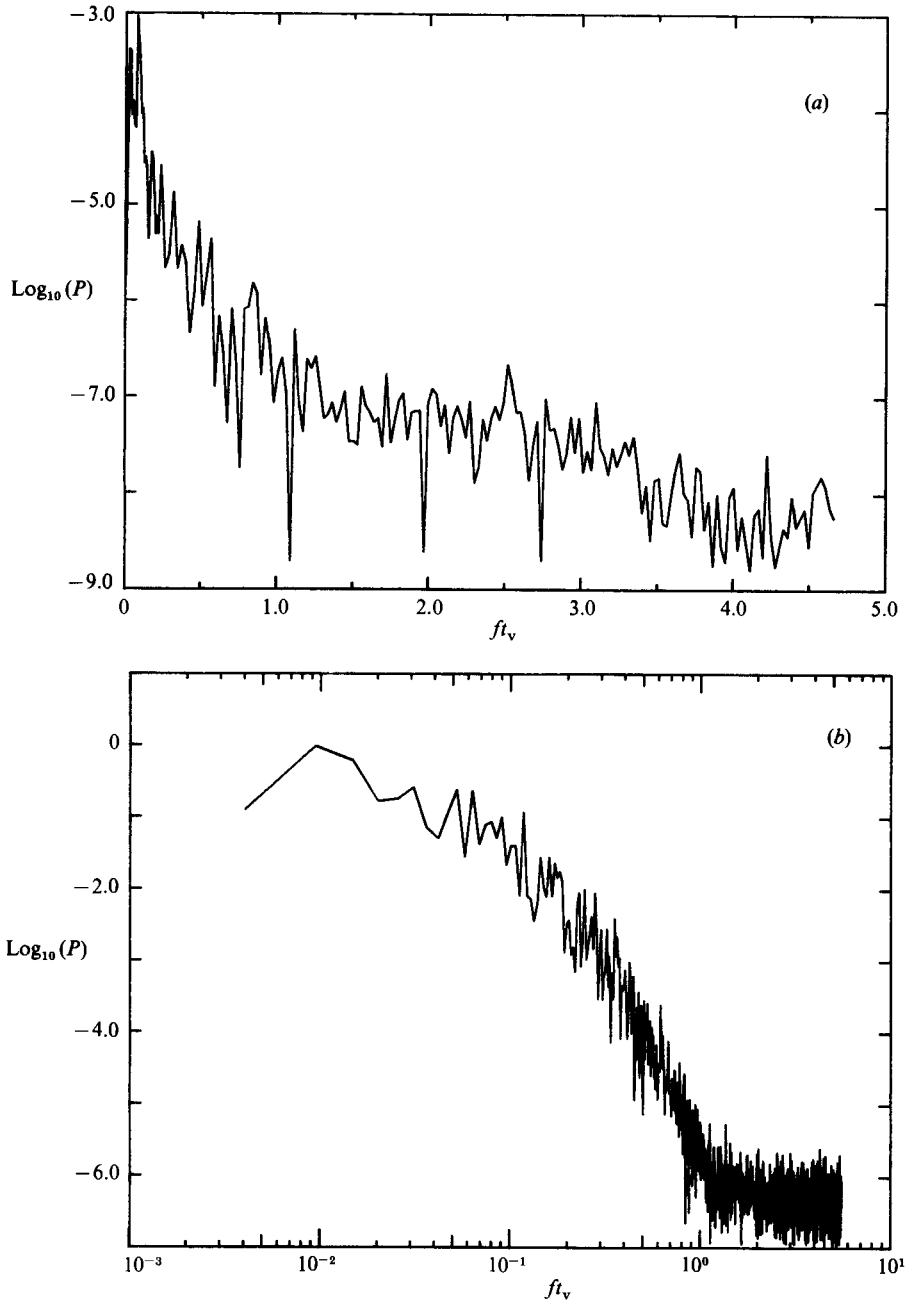


FIGURE 10. Power spectra for the time series of figure 9: (*a*) corresponds to 9(*a*) and (*b*) to 9(*b*).

It is interesting to compare spectra such as those of figure 10(*a*) to results obtained by Ahlers & Behringer (1978*a*, *b*) for liquid helium contained in a cylindrical geometry. Here, the aspect ratio was $\Gamma = 4.72$. In this case, after the onset of chaotic flow, a shoulder was also seen in the frequency range of the Busse and Clever predictions, superposed on a broadband spectrum. Some insight into this behaviour is provided by visualization studies by Pocheau *et al.* (1985). The fluid used in this case was argon gas with a Prandtl number of 0.69. Pocheau *et al.* found that the

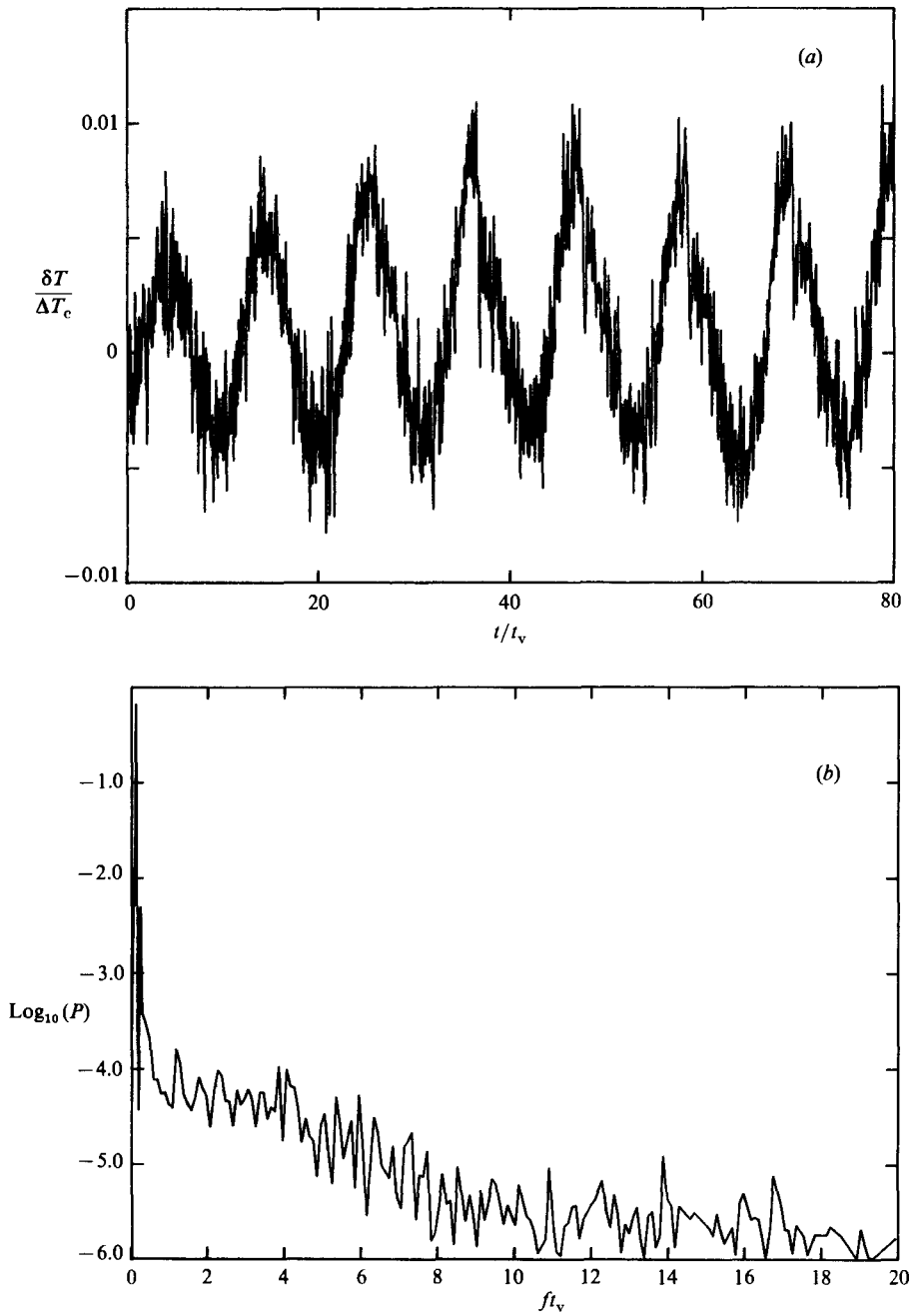


FIGURE 11. The onset of periodic flow in cell I: (*a*) a section of a time series at $3.39R_c$, and (*b*) the corresponding power spectrum.

oscillatory instability occurs locally where the wavevector is appropriate to the instability. We assume that such phenomena also occur in our rectangular containers.

By contrast, cell I showed two more episodes of time-dependent flow followed by steady flow before the onset of persistent time dependence at $R_5 = R_t$. Specifically, time dependence restarted at $R_3 = 3.39R_c$ as periodic flow (figure 11*a*). This periodic

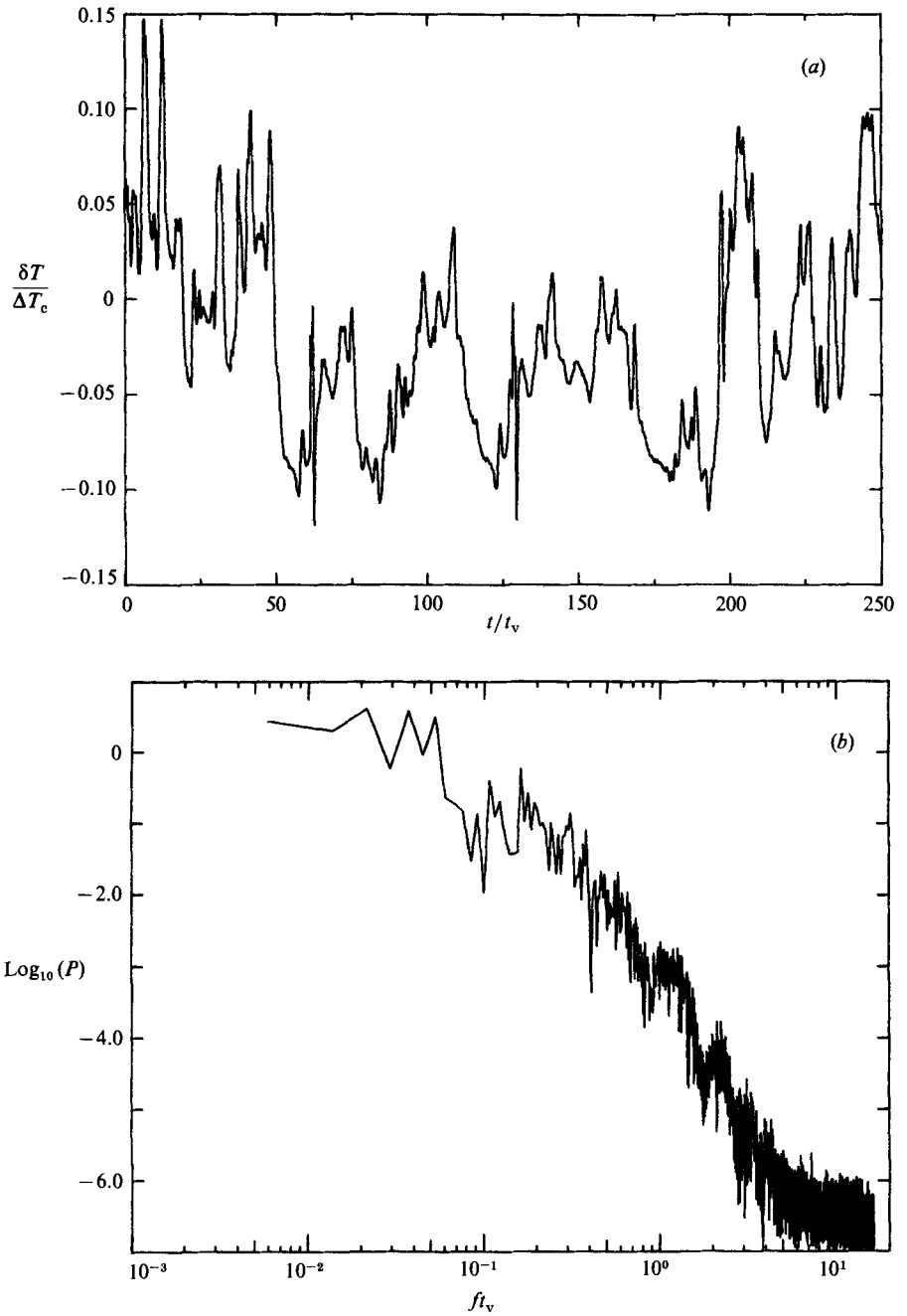


FIGURE 12(*a*,*b*). For caption see facing page.

flow, which occurs at a Rayleigh number that is appropriate to the predictions for the oscillatory instability, is qualitatively similar to what we have just considered for cell II at $R_t$. In particular, the dimensionless frequency was $9.22 \times 10^{-2}$, a value that is also about an order-of-magnitude lower than the theoretically expected value for the fastest-growing oscillatory mode on a set of rolls with $\alpha = 1.88$. The spectrum obtained from figure 11(*a*) is shown in figure 11(*b*). As for cell II, there is a knee at

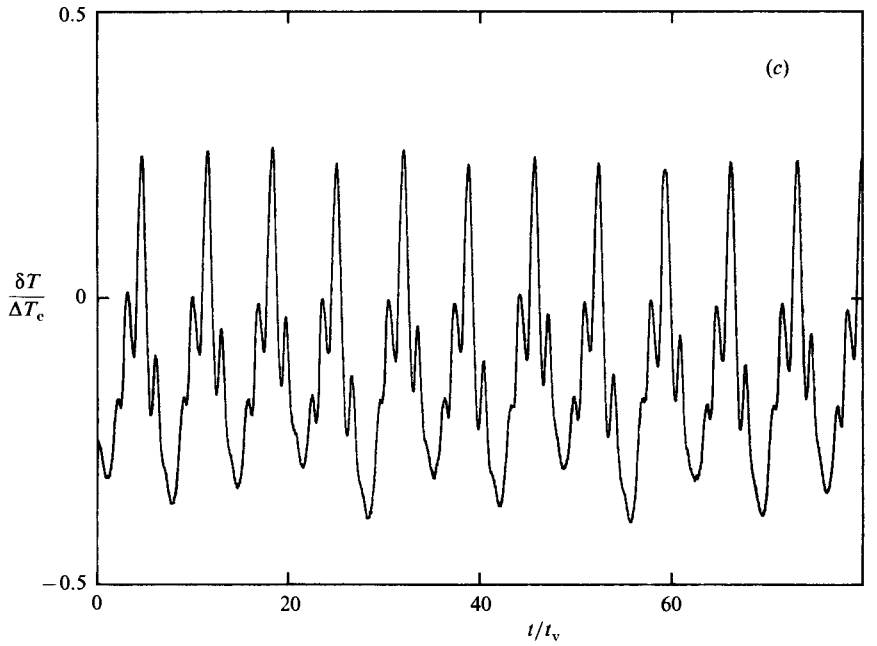


FIGURE 12. Time series and power spectra for cell I above $R_3$. (*a*) Non-periodic flow for cell I at $R = 4.30R_c$. (*b*) the power spectrum corresponding to (*a*); (*c*) a periodic state at $6.02R_c$.

a frequency that is appropriate to the oscillatory instability. In this case, the knee occurs at $ft_v \approx 5$. The periodic flow was found only over a narrow range and was replaced at $R = 3.55R_c$ by long transients corresponding to a time-monotonic increase of $R$ at fixed $Q$. These long transients were found up to $R_3^* = 3.85R_c$ where a narrow window, $3.85R_c < R < 4.06R_c$, of steady states existed which were characterized by rapid ($\sim$ a few $t_v$) relaxation times. At $R_4 = 4.06R_c$ non-periodic flow characterized by broadband spectra once again started (figure 12*a*, *b*). Between $4.06R_c$ and $6.68R_c$, the flow remained non-periodic with the exception of a complex periodic flow in the range $6.02R_c < R < 6.12R_c$ (figure 12*c*). This periodic state is reminiscent of the periodic flows reported by Ahlers & Walden (1980) and by Behringer *et al.* (1982) for cylindrical containers. At $R_4^* = 6.68R_c$, a band of steady states was again found extending up to $R_5 = R_t = 7.14R_c$. These states persisted for times up to $\approx 350\, t_v$ without decaying into a time-dependent state. In regard to this state, it is interesting to examine the integrated power

$$M_0 = \int P(\omega)\, \mathrm{d}\omega, \tag{9}$$

where $P$ is the power obtained from time variations $\delta T/\Delta T_c$ at fixed $Q$. Equivalently, $M_0$ is the variance of $\delta T/\Delta T_c$ in the time domain. $M_0$ is shown as a function of $R/R_c$ for the two cells in figure 13. For cell I, data for the region $6.68R_c \leqslant R \leqslant 7.14R_c$, indicated by the arrows in figure 13(*a*), are off the scale. Indeed, we did not detect any time dependence in that Rayleigh-number range, and the integrated power there, $M_0 = 2 \times 10^{-6}$, is due only to instrumental noise. As $R$ was increased above $7.14R_c$ in cell I, $M_0$ generally increased, although steady flow was found again at the single Rayleigh number $R = 8.13R_c$. By contrast, the integrated power for cell II increased steadily with $R$ above $2.53R_c = R_t$ for that container.

The steady flows found for $3.85R_c \leqslant R \leqslant 4.06R_c$, and particularly for $6.68R_c \leqslant$

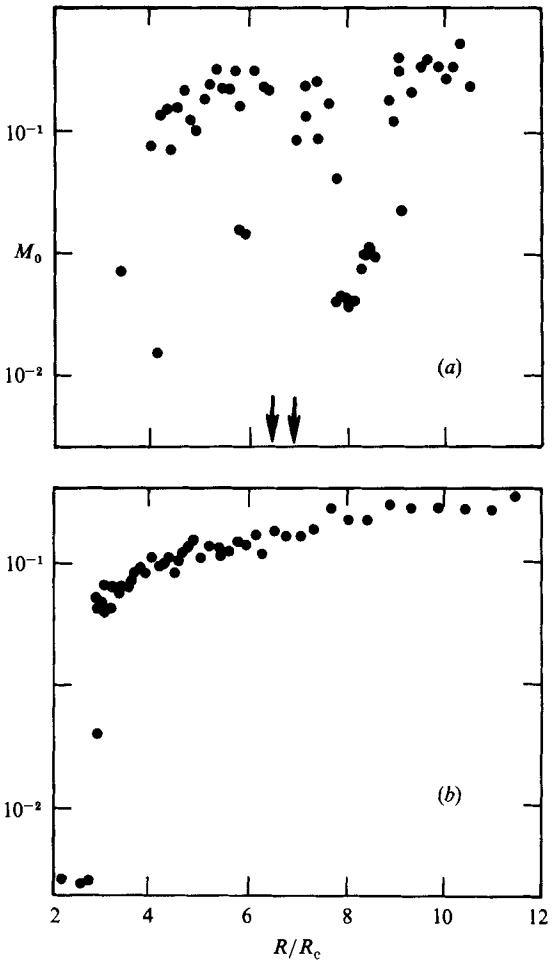


FIGURE 13. The zeroth moment of the power $M_0 = \int P(\omega)\,d\omega$: (*a*) cell I; (*b*) cell II. The arrows in (*a*) indicate the range over which the power has dropped to the long-time instrumental noise level of $2 \times 10^{-6}$, a level which would be off the scale of the figure.

$R \leqslant 7.14R_c$ and for $8.13R_c$ in cell I are surprising. In the stability analysis of Clever & Busse (1974) and Busse & Clever (1979), parallel rolls in a fluid of $Pr = 0.70$ are unstable to some instability regardless of $\alpha$ when $R \gtrsim 4R_c$, although once the stability boundaries have been crossed, time-dependence is not necessarily predicted. However, the experiments by Walden *et al.* (1984) and by Kolodner *et al.* (1986), with somewhat smaller horizontal dimensions than cell I, have not shown steady flow once the upper stability boundaries comparable with those in figure 1 have been crossed. Thus, we would have anticipated that the transition at $R_3$ with a wavenumber of $\alpha \approx 1.88$, would have placed the system outside the stable region and that thereafter no steady states should be observed.

## 4. Summary

These experiments have probed the onset of steady convection near $R_c$, the occurrence of secondary instabilities, and the onset of chaotic flow. Results near the onset of convection – the critical Rayleigh numbers and the initial slopes $N_1$ of the

Nusselt curve – are respectively in agreement with theory and comparable with results in moderate-aspect-ratio cylindrical containers. An investigation of the secondary instabilities shows transitions at Rayleigh numbers $R_1$ and $R_2$ that are in agreement with predictions for the skewed-varicose instability. These observations are also similar to results obtained with higher-Prandtl-number fluids. The next instability following $R_2$ was characterized by oscillations, as one would expect from the stability theories of Busse and Clever; however, the frequency was lower than these calculations suggest. Possibly, the depression in the frequency may be due to finite-size effects or to competition with the skewed-varicose instability. Further investigation, particularly with flow visualization, would be useful here.

A comparison of our data to the small-$L$ calculations of Kessler *et al.* (1984), Kessler (1987), and Yahata (1986, 1987) is also of interest. The Hopf bifurcation that Kessler *et al.* predict may correspond to the periodic states which we see briefly at $R_3$. However, in the calculations of Kessler, the periodic state is stable over a broad range of Rayleigh numbers. The difference between these calculations and our experiments may be attributed to the smaller container size assumed in the former ($L_x \times L_y = 4 \times 2$) and to the fact that roll-number changes do not occur in the former. In the calculations by Yahata, also for small $L_x$ and $L_y$, periodic states are likewise found. One of these in particular, the real mode instability, may be related to the experimental observations of state changes at $R_1$ and $R_2$. In the calculations, the original convection pattern becomes unstable to a real mode corresponding to a different pattern. However, there is no stable state associated with the new pattern, and a periodic state typically evolves instead. The differences between these calculations and the experiments seems to be that in the experiments, unlike the theory, a second stable state is available when the first state becomes unstable; consequently, the system eventually evolves to this second steady state. It seems possible that the availability of a nearby second state is related to the relatively large horizontal dimensions of the experiments.

Two other interesting observations remain to be explained. The first of these is the existence of apparently stable states at Rayleigh numbers well above those for which parallel rolls in an unbounded container are predicted to be unstable. It is unlikely that these steady states are characterized by straight rolls. We know of no previous experimental result that would have led us to expect their existence. The second unexplained observation of these experiments is the long timescales for the evolution of a new roll pattern following an encounter with the skewed-varicose instability. We find timescales that are of order $10^2 t_v$ or higher (i.e. comparable with or larger than $L_x^2 t_v$) for relaxation, whereas at higher Prandtl numbers the relaxation occurs over a timescale of $\approx t_v$.

This work has benefitted from discussions with Dr P. Kolodner, Dr C. Surko and Dr R. Walden. Support has been provided by the National Science Foundation under Low Temperature Physics Grant No. DMR-8314673.

## REFERENCES

AHLERS, G. 1974 Low temperature studies of the Rayleigh–Bénard instability and turbulence. *Phys. Rev. Lett.* **33**, 1185–1188.

AHLERS, G. & BEHRINGER, R. P. 1978*a* The Rayleigh–Bénard instability and the evolution of turbulence. *Prog. Theor. Phys. Suppl.* **64**, 186–201.

AHLERS, G. & BEHRINGER, R. P. 1978*b* Evolution of turbulence from the Rayleigh–Bénard instability. *Phys. Rev. Lett.* **40**, 712–716.

AHLERS, G., CANNELL, D. S. & STEINBERG, V. 1985 *Phys. Rev. Lett.* **54**, 1373.

AHLERS, G., CROSS, M. C., HOHENBERG, P. C. & SAFRAN, S. 1981 The amplitude equation near the convective threshold: application to time-dependent heating experiments. *J. Fluid Mech.* **110**, 297–334.

AHLERS, G. & REHBERG, I. 1986 Convection in a binary mixture heated from below. *Phys. Rev. Lett.* **56**, 1373–1376.

AHLERS, G. & WALDEN, R. W. 1980 Turbulence near onset of convection. *Phys. Rev. Lett.* **44**, 445–448.

BARENGHI, C. F., DONNELLY, R. J. & LUCAS, P. 1981 *J. Low Temp. Phys.* **44**, 491.

BEHRINGER, R. P. 1985 Rayleigh–Bénard convection and turbulence in liquid helium. *Rev. Mod. Phys.* **57**, 657–687.

BEHRINGER, R. P. & AHLERS, G. 1982 Heat transport and temporal evolution of fluid flow near the Rayleigh–Bénard instability in cylindrical containers. *J. Fluid Mech.* **125**, 219–258.

BEHRINGER, R. P., GAO, H. & SHAUMEYER, J. N. 1983 Time dependence in Rayleigh–Bénard convection with a variable cylindrical geometry. *Phys. Rev. Lett.* **50**, 1199–1202.

BEHRINGER, R. P., SHAUMEYER, J. N., CLARK, C. A. & AGOSTA, C. C. 1982 Turbulent onset in moderately large convecting layers. *Phys. Rev.* **A26**, 3723–3726.

BOLTON, E. W., BUSSE, F. H. & CLEVER, R. M. 1986 Oscillatory instabilities of convection rolls at intermediate Prandtl numbers. *J. Fluid Mech.* **164**, 469–485.

BUSSE, F. H. 1967 The stability of finite amplitude cellular convection and its relation to an extremum principle. *J. Fluid Mech.* **13**, 625–649.

BUSSE, F. H. 1981 Transition to turbulence in Rayleigh–Bénard convection. In *Hydrodynamic Instabilities and the Transition to Turbulence* (ed. H. L. Swinney & J. P. Gollub), pp. 97–137. Springer.

BUSSE, F. H. & CLEVER, R. M. 1979 Instabilities of convection rolls in a fluid of moderate Prandtl number. *J. Fluid Mech.* **91**, 319–335.

CHEN, M. E. & WHITEHEAD, J. A. 1968 Evolution of two-dimensional periodic Rayleigh convection cells of arbitrary wave-numbers. *J. Fluid Mech.* **31**, 1–15.

CLEVER, R. M. & BUSSE, F. H. 1974 Transition to time-dependent convection. *J. Fluid Mech.* **65**, 625–645.

CROSS, M. C. 1982 Ingredients of a theory of convective textures close to onset. *Phys. Rev.* **A25**, 1065–1076.

CROSS, M. C., DANIELS, P. G., HOHENBERG, P. C. & SIGGIA, E. D. 1983 Phase-winding solutions in a finite container above the convective threshold. *J. Fluid Mech.* **127**, 155–183.

GAO, H. & BEHRINGER, R. P. 1984 Onset of convective time dependence in cylindrical containers. *Phys. Rev.* **A30**, 2837–2839.

GAO, H., METCALFE, G., JUNG, T. & BEHRINGER, R. P. 1987 Heat-flow experiments in liquid $^4He$ with a variable cylindrical geometry. *J. Fluid Mech.* **174**, 209–231.

GOLLUB, J. P., MCCARRIER, A. R. & STEINMAN, J. F. 1982 Convective pattern evolution and secondary instabilities. *J. Fluid Mech.* **125**, 259–281.

GOLLUB, J. P. & STEINMAN, J. F. 1981 Doppler imaging of the onset of turbulent convection. *Phys. Rev. Lett.* **47**, 505–508.

KESSLER, R. 1987 Nonlinear transition in three-dimensional convection. *J. Fluid Mech.* **174**, 357–379.

KESSLER, R., DALLMANN, U. & OERTEL, H. 1984 Nonlinear transitions in Rayleigh–Bénard convection. In *Turbulence and Chaotic Phenomena in Fluids* (ed. T. Tatsumi), pp. 173–178. Elsevier.

KOLODNER, P., WALDEN, R. W., PASSNER, A. & SURKO, C. M. 1986 Rayleigh–Bénard convection in an intermediate-aspect-ratio rectangular container. *J. Fluid Mech.* **163**, 195–226.

KRICHNAMURTI, R. 1970 On the transition to turbulent convection. Part 1. The transition from two- to three-dimensional flow. *J. Fluid Mech.* **42**, 295–307.

KRISHNAMURTI, R. 1973 Some further studies of the transition to turbulent convection. *J. Fluid Mech.* **60**, 285–303.

LUCAS, P. G. J., PFOTENHAUER, J. M. & DONNELLY, R. J. 1983 Stability and heat transfer of rotating cryogens. Part 1. Influence of rotation on the onset of convection in liquid $^4He$. *J. Fluid Mech.* **129**, 251.

MAENO, Y., HAUCKE, H. & WHEATLEY, J. C. 1985 Transition to oscillatory convection in a $^3$He–$^4$He superfluid mixture. *Phys. Rev. Lett.* **54**, 340–342.

MAURER, J. & LIBCHABER, A. 1980 Effect of the Prandtl number on the onset of turbulence in liquid $^4$He. *J. Phys. Paris Lett.* **41**, 515–518.

NORMAND, C., POMEAU, Y. & VELARDE, M. 1981 Convective instability: a physicist's approach. *Rev. Mod. Phys.* **49**, 581–624.

PFOTENHAUER, J. M., LUCAS, P. G. J. & DONNELLY, R. J. 1984 Stability and heat transfer of rotating cryogens. Part 2. Effects of rotation on heat-transfer properties of convection in liquid $^4$He. *J. Fluid Mech.* **145**, 239–252.

POCHEAU, A., CROQUETTE, V. & LE GAL, P. 1985 Turbulence in a cylindrical container near threshold. *Phys. Rev. Lett.* **55**, 1095–1097.

STORK, K. & MÜLLER, U. 1972 Convection in boxes: experiments. *J. Fluid Mech.* **54**, 599–611.

WALDEN, R. W. 1983 Some new routes to chaos in Rayleigh–Bénard convection. *Phys. Rev.* **A27**, 1255.

WALDEN, R. W. & AHLERS, G. 1981 Non-Boussinesq and penetrative convection in a cylindrical cell. *J. Fluid Mech.* **109**, 89–114.

WALDEN, R. W., KOLODNER, P., PASSNER, A. & SURKO, C. M. 1984 Nonchaotic Rayleigh–Bénard convection with four and five incommensurate frequencies. *Phys. Rev. Lett.* **53**, 242–245.

WILLIS, G. E. & DEARDORF, J. S. 1970 The oscillatory motions of Rayleigh convection. *J. Fluid Mech.* **44**, 661–672.

WHITEHEAD, J. A. 1976 The propagation of dislocations in Rayleigh–Bénard rolls and bimodal flow. *J. Fluid Mech.* **75**, 715–720.

YAHATA, H. 1986 Evolution of convection rolls in low Prandtl number fluids. *Prog. Theor. Phys.* **75**, 790–807.

YAHATA, H. 1987 Competition of the two unstable modes in Rayleigh–Bénard convection. *Prog. Theor. Phys.* **78**, 282–304.